Earth and Planetary Science Letters 441 (2016) 103–112

Contents lists available at ScienceDirect

Earth and Planetary Science Letters

www.elsevier.com/locate/epsl

Pallasite paleomagnetism: Quiescence of a core dynamo

Claire I.O. Nichols [a,*], James F.J. Bryson [a,b], Julia Herrero-Albillos [c,d], Florian Kronast [e], Francis Nimmo [f], Richard J. Harrison [a]

[a] Department of Earth Sciences, University of Cambridge, Downing Street, Cambridge, CB2 3EQ, United Kingdom
[b] Department of Earth, Atmospheric and Planetary Sciences, Massachusetts Institute of Technology, 77 Massachusetts Avenue, Cambridge, MA 02139, USA
[c] Centro Universitario de la Defensa, Ctra. de Huesca s/n, E-50090 Zaragoza, Spain
[d] Instituto de Ciencia de Materiales de Aragón, CSIC—Universidad de Zaragoza, Pedro Cerbuna 12, E-50009 Zaragoza, Spain
[e] Helmholtz Zentrum Berlin, Elektronenspeicherring BESSY II, Albert-Einstein-Strasse 15, Berlin 12489, Germany
[f] Department of Earth Sciences, University of California Santa Cruz, CA 95064, USA

ARTICLE INFO

Article history:
Received 26 September 2015
Received in revised form 18 January 2016
Accepted 17 February 2016
Editor: B. Buffett

Keywords:
extraterrestrial magnetism
cloudy zone
pallasite meteorites
X-ray photoemission electron microscopy
core dynamo activity

ABSTRACT

Recent paleomagnetic studies of two Main Group pallasites, the Imilac and Esquel, have found evidence for a strong, late-stage magnetic field on the parent body. It has been hypothesized that this magnetic field was generated by a core dynamo, driven by compositional convection during core solidification. Cooling models suggest that the onset of core solidification occurred ~200 Ma after planetary accretion. Prior to core solidification, a core dynamo may have been generated by thermal convection; however a thermal dynamo is predicted to be short-lived, with a duration of ~10 Ma to ~40 Ma after planetary accretion. These models predict, therefore, a period of quiescence between the thermally driven dynamo and the compositionally driven dynamo, when no core dynamo should be active. To test this hypothesis, we have measured the magnetic remanence recorded by the Marjalahti and Brenham pallasites, which based on cooling-rate data locked in any magnetic field signals present ~95 Ma to ~135 Ma after planetary accretion, before core solidification began. The cloudy zone, a region of nanoscale tetrataenite islands within a Fe-rich matrix was imaged using X-ray photoemission electron microscopy. The recovered distribution of magnetisation within the cloudy zone suggests that the Marjalahti and Brenham experienced a very weak magnetic field, which may have been induced by a crustal remanence, consistent with the predicted lack of an active core dynamo at this time. We show that the transition from a quiescent period to an active, compositionally driven dynamo has a distinctive paleomagnetic signature, which may be a crucial tool for constraining the time of core solidification on differentiated bodies, including Earth.

1. Introduction

Paleomagnetic studies of meteorites provide evidence that core dynamos were a widespread feature of planetesimals during the early solar system (Weiss and Elkins-Tanton, 2013; Scheinberg et al., in press). Two recent studies (Tarduno et al., 2012; Bryson et al., 2015) have shed light on the nature of magnetic fields on the Main Group (MG) pallasite parent body. Time-resolved paleomagnetic records suggest the MG parent body experienced an intense, late-stage magnetic field, which is attributed to an active core dynamo driven by compositional convection during inner core solidification (Nimmo, 2009). The onset of core solidification is predicted to have started ~190 Ma after planetary accretion, based on the planetary cooling model proposed by Bryson et al. (2015) for a 200-km-radius body. Prior to this time, any long-term dynamo would have been driven by thermal convection. Thermal modelling suggests an active thermal dynamo would require a magma ocean to generate the required heat flux out of the core. This is predicted to have acted at most for 10–40 Ma after accretion (Elkins-Tanton et al., 2011), leading to a quiescent period after the shut down of the thermal dynamo and before the onset of core solidification. A thermal dynamo requires a high heat flux to operate and therefore tends to be of limited duration. Numerical modelling and simple energy balance arguments suggest that a small planetary body with radius <500 km cannot be sustained for more than 10 Ma (Sterenborg and Crowley, 2013). These authors demonstrate that the lifetime of a thermal dynamo is highly dependent on the radius of the planet, $t_{dyn} \propto r^4$, therefore other physical parameters (such as convection of a magma ocean) have an insignificant effect on dynamo duration compared to planetary radius. Likewise, a compositionally driven dynamo can only become active after suf-

* Corresponding author.
E-mail address: cion2@cam.ac.uk (C.I.O. Nichols).

http://dx.doi.org/10.1016/j.epsl.2016.02.037

ficient cooling of the planetary body has taken place for the core to reach its liquidus temperature. Here we investigate if any magnetic field was generated by, or acting on, the MG parent body between these predicted periods of dynamo activity.

In the following, we follow Tarduno et al. (2012) in assuming that the metallic component of the MG pallasites was delivered to the pallasite parent body during a collision with another differentiated body. The metal will have rapidly solidified and thermally equilibrated with the surrounding silicates; the cooling rates thereafter would have been controlled by the depth of metal within the parent body. Pallasites with different cooling rates are assumed to have experienced different long-term thermal evolution, owing to their differing depths within the parent body. For consistency with prior work, we assume the same pallasite parent body radius (200 km) to derive original depths based on the observed metallographic cooling rates. Small variations in the size of the parent body do not significantly affect the timing of magnetisation for the pallasites, so do not change our results (see Supplementary Table 1).

Two MG pallasites, the Brenham and Marjalahti, have been measured to study the possible presence of magnetic fields during the predicted quiescent period. Both pallasites were examined for paleomagnetic signals recorded by microstructures within the FeNi matrix. New experimental techniques such as electron holography (Bryson et al., 2014a) and X-ray photoemission electron microscopy (X-PEEM) (Bryson et al., 2014b), have revealed the capability of meteoritic FeNi metal to record information about these ancient paleomagnetic fields. The FeNi metal contains a range of microstructures depending on its local Ni content. During slow cooling, nucleation of kamacite lamellae within the parent taenite leads to the characteristic Widmanstätten pattern and distinctive M-shaped diffusion profiles (Yang et al., 1996). Local Ni composition within the M-shaped profile varies from ∼50% bulk Ni content immediately adjacent to the kamacite lamellae to ∼10% further away from the kamacite interfaces. The most Fe-rich phase is kamacite, which forms intersecting μm-scale lamellae. These lamellae contain multiple magnetic domains and are magnetically soft, making them poor paleomagnetic recorders (Garrick-Bethell and Weiss, 2010). Adjacent to the kamacite is the tetrataenite rim ($Fe_{0.5}Ni_{0.5}$), a 1–2 μm-wide region which also exhibits multidomain magnetic behaviour. Next to the tetrataenite rim is the 'cloudy zone', which is followed by plessite; a mixture of kamacite, taenite and ordered tetrataenite (Goldstein and Michael, 2006).

The 'cloudy zone', a region of $Fe_{0.5}Ni_{0.5}$ 'islands' in a Fe-rich matrix, forms by spinodal decomposition during slow cooling of FeNi metal with composition ∼25–45% Ni (Yang et al., 2010). The size of the islands correlates inversely with cooling rate (Yang et al., 2010); once islands form they then continue to coarsen and their volume increases linearly over time (at constant temperature) (Weinbruch et al., 2003). The islands are formed of ordered tetrataenite with the tetragonal $L1_0$ superstructure (Yang et al., 1996). This structure means that they are excellent paleomagnetic recorders, with an intrinsic coercivity of ∼2 T (Uehara et al., 2011). The c-axis is perpendicular to one of the three {100} orientations of FeNi layering (Lewis et al., 2014) providing three orthogonal easy axes along which the islands can be magnetised. As the cloudy zone forms, the atomic structure adopted by each island will be influenced by the presence of any magnetic field, locking in a chemical transformation remanent magnetisation (CTRM). If the cloudy zone forms in the absence of an external field, the islands within the cloudy zone will be magnetised along each of six possible directions (± directions along each of the three easy axes); however in the presence of an external field, a bias in the direction of magnetisation can be detected. This bias can be used to quantify the magnetic field intensity experienced by the cloudy zone at the time when magnetisation became locked in. The islands lock in a magnetic field signal when they reach their blocking volume (the volume at which the magnetisation of the island becomes stable), so the largest islands lock in paleomagnetic signals earlier than the smaller islands (they have coarsened more since growing through their blocking volume). The blocking volume is reached when the island size exceeds the diffusion length, preventing reorganisation of easy axes and hence magnetisation across the entire island. The island may continue to grow and coarsen after this time, but the magnetisation of each island is expected to remain constant.

We chose the Brenham and Marjalahti based on the size of the islands in the cloudy zone, which at their coarsest are 123 ± 3 nm and 118 ± 3 nm in diameter, respectively (Yang et al., 2010). The coarsest islands in the Imilac and Esquel, which revealed evidence for a compositionally driven dynamo (Bryson et al., 2015; Tarduno et al., 2012) are 143 ± 4 nm and 157 ± 11 nm; since these two pallasites cooled slower, they are predicted to have reached the cloudy zone formation temperature later and hence have recorded a later period of dynamo activity than the Brenham and Marjalahti. According to the thermal model for the MG pallasite parent body, the Brenham and Marjalahti formed their cloudy zones and acquired a CTRM prior to the onset of inner core solidification. Constraining paleomagnetic signals in this potentially quiescent period is essential for characterising core dynamo behaviour over long timescales, and may help with identifying signals that indicate the onset of core solidification.

2. Methods

2.1. Experimental methods

Samples of the Brenham (BM 68725) and Marjalahti (BM 1920,318) were obtained from the Natural History Museum, London, UK. The samples were initially polished and etched using nital (2% nitric acid in ethanol) and examined using a reflected light microscope to check for signs of alteration or shock. Samples were then repolished to reveal a fresh surface prior to X-PEEM measurements. X-PEEM was performed at the SPEEM UE49 beamline, BESSY II, Berlin (Kronast et al., 2010). Firstly, the samples were sputtered using a focused Ar-ion beam under vacuum (pressure $<1.5 \times 10^{-5}$ mbar) to remove any oxidation or surface magnetisation induced by polishing. The Marjalahti was sputtered for 20.5 h and the Brenham for 19 h whilst reducing the voltage from 1.2 keV to 0.4 keV to minimise surface topography due to differential etching. The samples were kept in vacuum after sputtering and prior to measuring (measuring pressure $<1 \times 10^{-8}$ mbar). X-PEEM images with a 5 μm field of view were taken at multiple locations around the Marjalahti and Brenham. The maximum possible resolution achievable with this technique is 30 nm (Locatelli and Bauer, 2008), although resolution varies depending on several factors. An intense beam of monochromatic X-rays was focused at an angle of 16° to the sample surface. Secondary photoelectrons were excited from the top ∼5 nm of the sample surface by the X-rays. Photoelectrons are preferentially excited from particular elements and spin states, according to the energy and polarisation of the X-ray beam, respectively. Excited photoelectrons were accelerated and focused using electron lenses, forming an image of the sample surface (Ohldag et al., 2001; Nolting et al., 2000). This technique allows compositional and magnetic imaging to be carried out in the same location in quick succession by changing the energy and polarisation of the X-ray beam, meaning a direct comparison can be made between composition and magnetisation for each region. Each image is individually assessed for light drift and charging artefacts, and only the highest quality data are selected for further analysis.

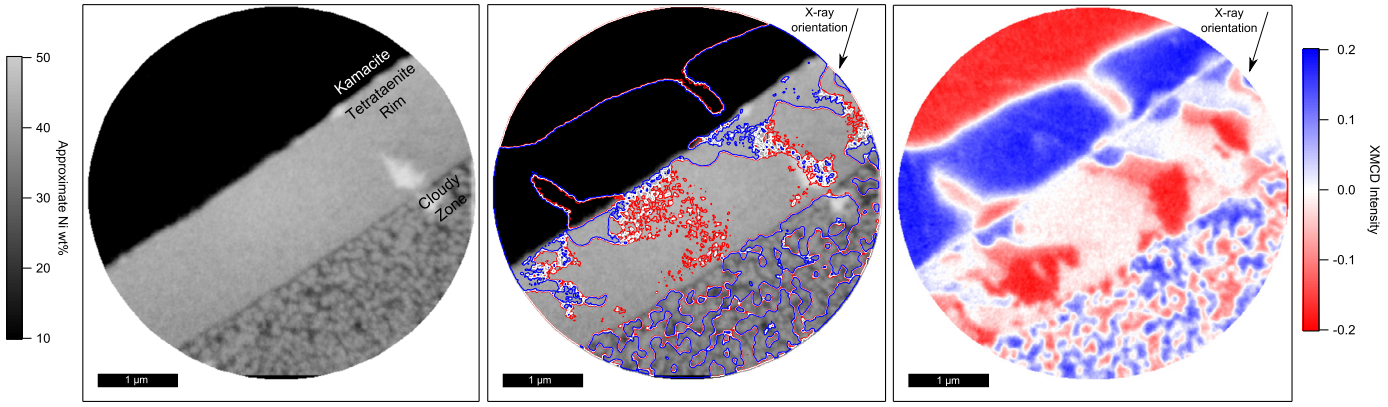

Fig. 1. From left to right: A compositional image of the kamacite, tetrataenite rim and cloudy zone from the Marjalahti. Approximate Ni composition is given, under the assumption that the tetrataenite rim has a composition $Fe_{0.5}Ni_{0.5}$. The middle image shows the composition overlain with the magnetisation as it changes from positive to negative. It can clearly be seen that the behaviour changes abruptly at the microstructural boundaries. The kamacite and tetrataenite rim both exhibit large, multidomain magnetisation, whereas in the cloudy zone the magnetisation becomes clustered around the tetrataenite islands. On the right is the magnetic image of the same region for comparison. N.B. The pale region on the right of the compositional images represents dust on the sample surface, and is not a genuine reflection of composition.

2.1.1. Compositional images

Compositional images were acquired using linearly polarised X-rays tuned to the Fe L_3 and Ni L_3 energies (707 eV and 852 eV, respectively). Images were also acquired at pre-edge energies (700 eV and 845 eV for Fe and Ni, respectively). Each on-edge image was normalised by dividing by its equivalent pre-edge image. The Ni image is divided by the Fe image in order to generate a semi-quantitative map of Ni/Fe ratios.

2.1.2. Magnetic images

X-ray magnetic circular dichroism (XMCD) was used to image the magnetisation state at the Fe L_3 edge (Ohldag et al., 2001; Stöhr et al., 1998). Images were acquired for both left and right circularly polarised X-rays, which excite electrons in opposite spin states. Since spin state directly correlates to the direction of magnetisation, this generates contrast depending on the component of magnetisation parallel to the X-ray beam. Images were taken along parallel sections of the tetrataenite rim in order to be directly comparable. Images taken in each polarisation state were subtracted from one another and divided by their sum, in order to normalise and enhance magnetic contrast.

2.2. Image interpretation and analysis

Compositional images were used to constrain the boundaries between the different microstructures, in particular the boundary between the tetrataenite rim and the cloudy zone. The relationship between composition and magnetisation was examined qualitatively, either by overlaying contours of zero magnetic intensity (corresponding to the boundaries between positively and negatively magnetised domains) or by overlaying traces of sharp boundaries in Ni content on magnetic images (Fig. 1).

The cloudy zone was split into discrete regions with decreasing island size. XMCD values from each region were compared quantitatively to those of a simulated nanostructure, generated using procedures outlined by Bryson et al. (2014b). The simulated images were created by generating a nanostructure comprised of 800 islands, by eroding Voronoi cells (Fig. 2e). The pixel size was adjusted in order to give the islands comparable dimensions to those in the experimental images. The matrix was assumed to be strongly exchange-coupled to the closest islands and therefore adopts the same XMCD value (Fig. 2f). The resolution for each simulated image is calculated by taking multiple line profiles of XMCD value across a boundary between two islands in the experimental XMCD images. The resolution is directly related to the pixel width of the boundary between island and matrix. A representative degree of noise is also added to simulated images.

Quantitative comparisons are made by assessing similarities between the experimental and simulated histograms of pixel intensity for each region. 9 and 12 simulations of the Brenham and Marjalahti, respectively, were run to reflect the number of images attained experimentally. Simulations were performed for a range of applied magnetic fields and directions. The direction of the applied magnetic field was constrained along the three orthogonal easy axes, defined by the L_{10} superstructure; a combination of these 3 axes can generate a 3D vector of the magnetic field in any direction. The strength of the applied field is simulated by preferentially biasing the probability of islands having one of the three intensities defined by each easy axis. The simulations assume that the remanence acquired by the islands is a CTRM rather than a thermal remanent magnetisation (TRM). The mechanism by which islands acquire there remanence is currently poorly understood, however Bryson et al. (2015) assume a CTRM for their simulations, and this gives good agreement with magnetic field values from independent paleomagnetic studies of pallasite olivine crystals (Tarduno et al., 2012). The magnetic intensity associated with each easy axis direction is derived from the values present in the tetrataenite rim.

Bootstrapping, a statistical technique used to calculate the confidence level of a distribution, was applied to both the experimental and simulated results to find an agreement between the two to >95% confidence (DiCiccio and Efron, 1988). Histograms of pixel intensity are normalised to probability density functions, the integral of each function is then calculated and plotted against its respective XMCD value (Supplementary Fig. 1). The integrated curve was then randomly sampled 201 and 218 times for the Brenham and Marjalahti respectively (the predicted minimum number of islands present in each analysed region). The random sampling of the curve generates a new, resampled distribution of magnetic intensity for each image. A mean and standard deviation were then calculated for the resampled distribution. This process was repeated 1000 times to generate results with a statistically significant confidence level, in order to build up a distribution of the mean pixel intensity for each image. The distributions of the means can then be compared for the experimental and simulated images, in order to constrain an upper and lower bound on magnetic field strength experienced by the samples.

The relative age at which each of the samples was magnetised was calculated using the cooling model for a 200 km radius body (Supplementary Table 1) with a 100 km radius core (Tarduno et al., 2012). The core is taken to be half the radius of the parent body,

since this represents the ratio of metal to silicates in the solar nebular, and also reflects the relative size of the Earth's core. However, this is not to say that the core cannot be larger or smaller and it must be acknowledged that this would change the size of the parent body significantly. The cooling rate of the Brenham and Marjalahti at 800 K is calculated from the reported size of the tetrataenite islands in the cloudy zone immediately adjacent to the tetrataenite rim using

$$d_{CZ}^{2.9} = \frac{k}{CR} \quad (1)$$

where d_{CZ} is the diameter of islands in the cloudy zone in nm, k is a constant, equal to 7,620,000 K nm Ma^{-1} and CR is the cooling rate in K Ma^{-1} (Yang et al., 2010). Cooling rates were calculated to be 6.6 ± 0.5 K Ma^{-1} for Brenham and 7.6 ± 0.6 K Ma^{-1} for Marjalahti. The cooling rate for the Brenham has also been directly measured from its M-shape Ni profile to be 6.2 ± 0.9 K Ma^{-1} (Yang et al., 2010), showing good agreement with our calculated value. The cooling rate can then be converted to a depth within the pallasite parent body, based on the calculated cooling rate for a 200 km radius body. The critical ordering temperature for tetrataenite is 320 °C; it is assumed Brenham and Marjalahti acquire ambient magnetisation at the time when they cool through this temperature. The Marjalahti and Brenham formed at depths of 22 ± 1.5 km and 24 ± 1.5 km, respectively and their cloudy zones formed ~95–114 Ma and ~112–135 Ma after accretion.

3. Results and implications

3.1. Comparison of composition with magnetisation

Images of magnetisation and composition were acquired for several regions of the Marjalahti in order to examine the relationship between the two. The contrasting magnetic behaviour of each microstructure is immediately apparent (Fig. 1). The large kamacite lamellae consist of many large (~1–5 μm) magnetic domains which exhibit multidomain behaviour (Garrick-Bethell and Weiss, 2010). The tetrataenite rim also shows multidomain magnetic behaviour, however here the magnetic domains are smaller (typically on the order of the width of the tetrataenite rim). The cloudy zone displays contrasting magnetic behaviour; magnetic domains are clearly observed to be clustered around regions of tetrataenite islands and Fe-rich matrix (Fig. 2). There is no clear relationship between magnetic intensity and the transition from island to matrix, although in general, the islands appear to have slightly higher XMCD intensities.

The multidomain magnetic behaviour of both the kamacite and the tetrataenite rim suggests both are poor paleomagnetic recorders. In the cloudy zone, there is unequivocal evidence that both islands and matrix constitute a continuous magnetic structure, i.e. the matrix is not paramagnetic antitaenite, as suggested by previous Mössbauer experiments (Dos Santos et al., 2015). Note, however, that the domain walls occur predominantly in the matrix rather than intersecting islands. This is consistent with magnetically hard, single domain islands surrounded by magnetically soft matrix. This pattern is in agreement with the predicted formation of the cloudy zone by spinodal decomposition (Yang et al., 2010; Bryson et al., 2014a). The islands and matrix are magnetically connected by exchange coupling; if the matrix were paramagnetic, then the boundary between islands and matrix would have zero magnetic intensity (white). The magnetic clustering of islands and matrix (where clustering describes the increased probability that an island will be magnetised in the same direction as its immediate neighbours) supports the matrix having ferromagnetic behaviour, consistent with a phase of ordered $Fe_{0.75}Ni_{0.25}$ as suggested by Bryson et al. (2014b).

3.2. Quantification of paleomagnetic field values

12 and 9 sets of parallel XMCD images were taken for the Brenham and Marjalahti, respectively. Histograms of pixel intensity were generated for 4 adjacent regions in the Brenham and 5 in the Marjalahti, where each region is parallel to, and progressively moving away from, the tetrataenite rim. The number of regions is constrained by the amount of cloudy zone present in each image and does not reflect genuine differences in the width of the cloudy zone between the two meteorites. The histogram peaks for both the Brenham and Marjalahti show very small offsets from zero; much smaller than those observed for the Imilac and Esquel. The distributions are also much closer to being symmetric than those for the Imilac and Esquel. In all cases the offset is consistently in the same direction (Supplementary Fig. 2).

The maximum island size, reported by Yang et al. (2010) for the Brenham (123 ± 3 nm) and the Marjalahti (118 ± 3 nm) was used in order to estimate the critical blocking volume of the islands, at which point they record their magnetic field. This is taken to be ~0.3 times their present-day size (37 nm for the Brenham and 35 nm for the Marjalahti) based on comparison of fields obtained by Bryson et al. (2015) with those of Tarduno et al. (2012) for the MG pallasites. Uncertainty in this value provides the greatest uncertainty in the absolute value of magnetic field. Nevertheless, relative comparisons between samples with similar island sizes remains valid. Increasing the blocking volume would lead to a decrease in the field, and vice-versa. The resolution of the XMCD images was calculated to be ~110 nm for Brenham, and ~130 nm for Marjalahti.

The distributions of means (calculated using bootstrapping) for both the experimental and simulated histograms are plotted for zero ambient field and the maximum ambient field (Figs. 3 and 4). Results can all be explained by a weak ambient magnetic field between ~1 and ~7 μT; however many regions lie within 2σ of a 0 μT field (the 95% confidence interval), whilst the rest lie on the edge or just outside of the 2σ range, therefore the absence of an ambient field cannot be discounted.

Results for the Marjalahti and Brenham can then be compared to those for the Esquel and Imilac as calculated by Bryson et al. (2015) (Fig. 5). The offsets in pixel intensity for the Brenham and Marjalahti can be accounted for by significantly weaker magnetic field signals (~1–7 μT) compared to the offsets experienced by the Imilac (~119–131 μT) and the Esquel (~31–84 μT) (Supplementary Table 2). The exception is the final region of the Esquel, which has a much more symmetric distribution in pixel intensity and can be explained by a field of ~0–10 μT.

3.3. Paleomagnetic signals recorded by the Brenham and Marjalahti and their implications for core dynamo activity

A new formation mechanism was required for the pallasites after a number of lines of evidence demonstrated that they were unlikely to originate from a core–mantle boundary. It has recently been proposed that the MG pallasite parent body formed by an impact that injected the molten metallic core of one planetesimal into the silicate mantle of the other, forming downward intruding, metallic dykes (Tarduno et al., 2012; Reimold and Gibson, 2006). This formation mechanism is supported by modelling that demonstrates how 'hit and run' collisions between two small planetary bodies can lead to mixing of the core of one body and the mantle of the other (Asphaug et al., 2006). It is also supported by the observation of a paleomagnetic remanence within the Imilac and Esquel samples, which is considered to have been imparted by the presence of core dynamo fields. Since core dynamo generation requires at least a partially molten core, core temperatures must have exceeded 1200 K (Tarduno et al., 2012), while the cloudy

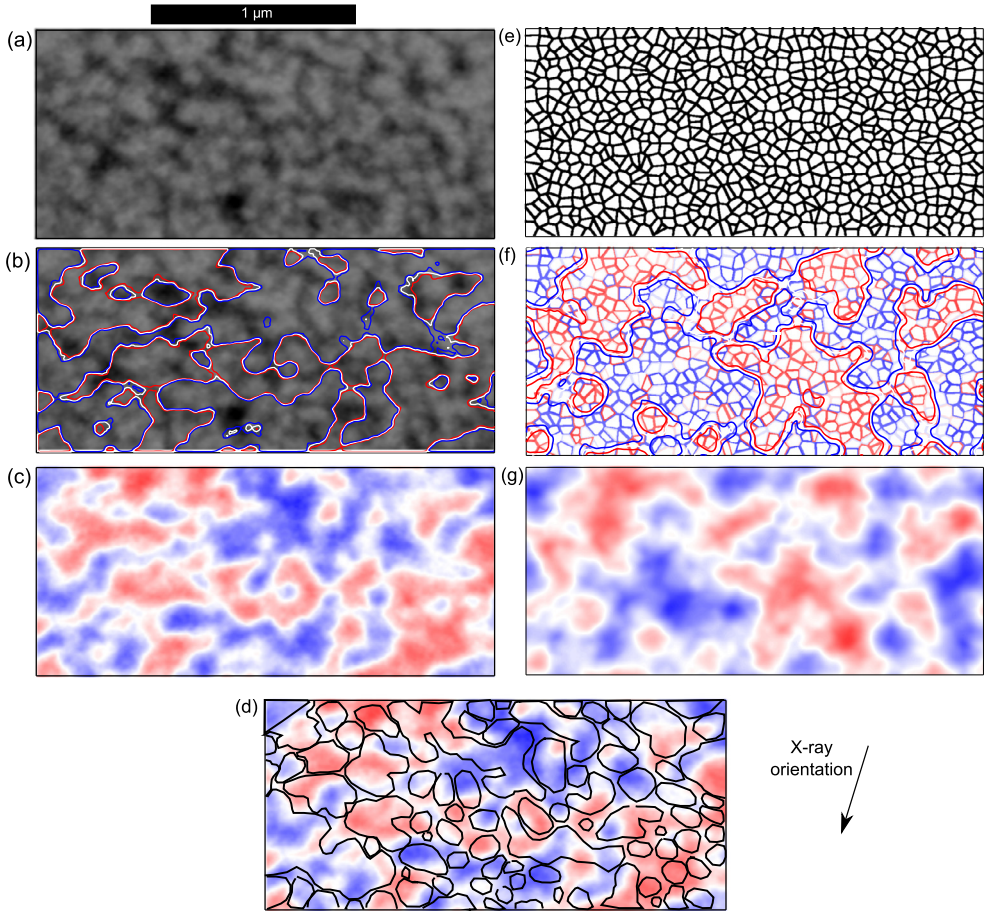

Fig. 2. (a) Compositional image of the cloudy zone in the Marjalahti palasite. Paler regions represent tetrataenite islands, whilst darker regions represent Fe-rich matrix. (b) An overlay of the location of the magnetic domain walls on the compositional image. This emphasises how the magnetisation clusters around the islands. The colours represent the direction of magnetisation relative to the X-ray beam; red indicates magnetisation towards the beam, white perpendicular to the beam and blue away from the beam. (c) The magnetisation of the same region of the cloudy zone. Again, the clustering of magnetic domains around the tetrataenite islands is evident. (d) The approximate compositional boundary between islands and matrix overlain on the XMCD image of magnetisation. (e) Simulated cloudy zone islands, generated by erosion of Voronoi cells. (f) The matrix is assigned an XMCD value depending on the magnetisation of the surrounding islands. Island XMCD values are influenced by the applied magnetic field and the degree of clustering in the experimental XMCD image. The six possible values of XMCD intensity for each island are derived from the observed intensities in the tetrataenite rim. This is overlain with contours showing the position of domain walls in the final simulated image, shown in (g). (g) Simulation of the XMCD image, taking into account the resolution and noise of the experimental image. (For interpretation of the references to color in this figure legend, the reader is referred to the web version of this article.)

zone does not form until temperatures $<400\,^{\circ}C$, suggesting the pallasites must have formed at a much shallower depth in the parent body. Geochemical analysis also suggests that the FeNi metal and olivine crystals are not from the same source (Hsu, 2003).

Our X-PEEM observations provide clear evidence that the Brenham and Marjalahti recorded highly contrasting paleomagnetic signals to the Imilac and Esquel, resulting from very different magnetic field regimes. Maximum field values calculated for the Brenham and Marjalahti do not exceed ~10 μT. The variability in maximum applied magnetic field for each region of the Marjalahti and Brenham is interpreted as reflecting the larger degree of uncertainty on the paleomagnetic field signal; values are not well resolved enough to say with any certainty if there are genuine small degrees of variability, therefore the Marjalahti and Brenham are interpreted to have experienced a small, weak, stable magnetic field. Figs. 3 and 4 show a consistent offset direction from zero across all regions for both samples. This rules out the possibility of the observed weak field being the result of averaging multiple magnetic reversals within each sampled time period. In the case of magnetic field reversals, the bias in XMCD intensity would be expected to vary between regions. The following discussion of magnetic field strengths is based on a very conservative interpretation of the data; the variability and specific upper bound on the paleomagnetic field signal become irrelevant for interpreting our results in a broader context and discussing likely core dynamo behaviour.

The Imilac records an intense dipolar magnetic field whilst the Esquel records decay to a weak, multipolar field. The final stage of this decay has a comparable magnetic field strength to that experienced by the Marjalahti and Brenham. The initial intense field has been interpreted to represent a dipolar dynamo field, generated by compositional convection during core solidification. Compositional convection is promoted by the presence of lighter elements (such as S) in the core, which are incompatible and hence preferentially partition into the outer, liquid part of the core (Chabot, 2004). The Brenham and Marjalahti may have recorded a weak magnetic field, which could be interpreted as the onset of a compositionally-driven dynamo. This is unlikely for two reasons. First, the Brenham and Marjalahti are predicted to record a field prior to the onset of core solidification so there is no buoyancy flux to initiate a compositionally-driven core dynamo (Nimmo, 2009). Second, there is no indication of an increase of field over time, which would be necessary to link to the magnetic field recorded by the Imilac; neither the Brenham nor the Marjalahti show any evidence for a significant increase in magnetic field. A mechanically driven dynamo is ruled out since the pallasite parent body is unlikely to

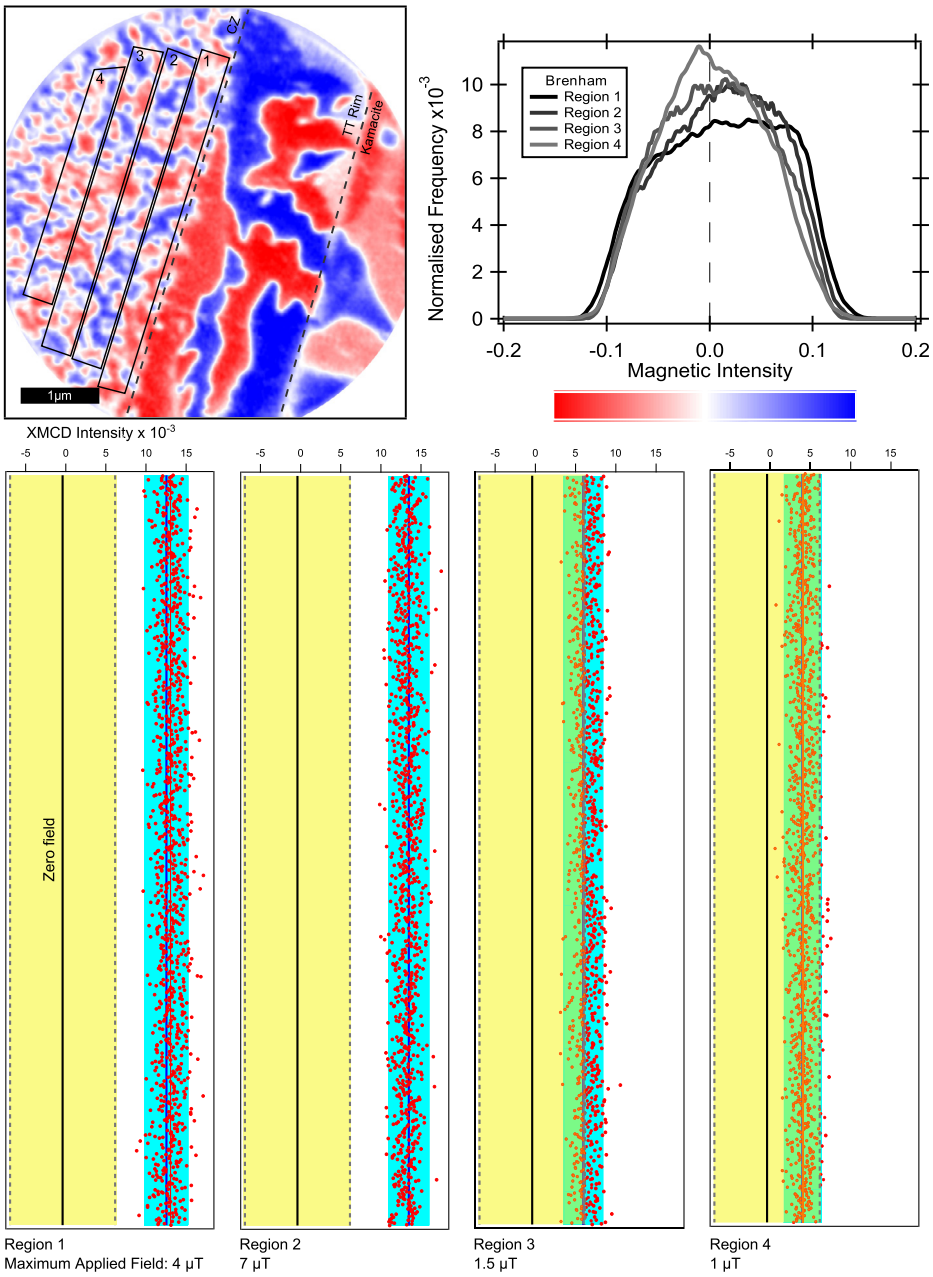

Fig. 3. An XMCD image for the Brenham shows the four regions analysed. The histogram shows the pixel intensity for the average of the 9 experimental images acquired and analysed. The lower four plots are the results of bootstrapping analysis. The black line represents a simulation under zero ambient field. The yellow area represents 2 standard deviations, and hence describes a zero ambient field to a confidence level of 95%. The red dots represent the mean of the experimental histograms, resampled 1000 times. The blue line is the best fit to the experimental data, acquired by varying the ambient magnetic field. The pale blue region is the 95% confidence level for the maximum field fit. The maximum fit for each region is reported underneath each graph. (For interpretation of the references to colour in this figure legend, the reader is referred to the web version of this article.)

have had a companion large enough to drive precession (Dwyer et al., 2011) and an impact-driven dynamo would be associated with sudden peaks in magnetisation, rather than a constant field (Le Bars et al., 2011). The magnetic field captured by Brenham and Marjalahti appears to be sustained for at least ~40 Ma.

The presence of a small constant magnetic field could be caused by a crustal remanence, induced by an early stage thermal dynamo. Simple thermal modelling (Elkins-Tanton et al., 2011) suggests a magma ocean could have been sustained for a maximum of 17 Ma on the pallasite parent body, acting as the driving force for a short-lived thermal dynamo (see Supplementary Information). In order to test the likelihood of a weak magnetic field generated by a crustal remanence, we used Runcorn's theorem (Runcorn, 1975) to calculate the magnitude of an internal magnetic field generated by a crustal remanence, assuming an idealised, spherical body with a crust of uniform thickness that was magnetised by a dipolar field. The internal field strength is given by

$$B_{internal} = \frac{2\mu_o}{r^4}\chi_{TRM} t_{crust} M_{dyn} \quad (2)$$

where μ_0 is the magnetic permeability of free space, $r = 200$ km is the radius of the body and χ_{TRM} is the crustal magnetic susceptibility (for derivation see Supplementary Information). The magnetic crustal thickness, t_{crust}, was varied from 0 to 20 km; 20 km is predicted to be the maximum thickness of material that would have cooled through its Curie temperature and become magne-

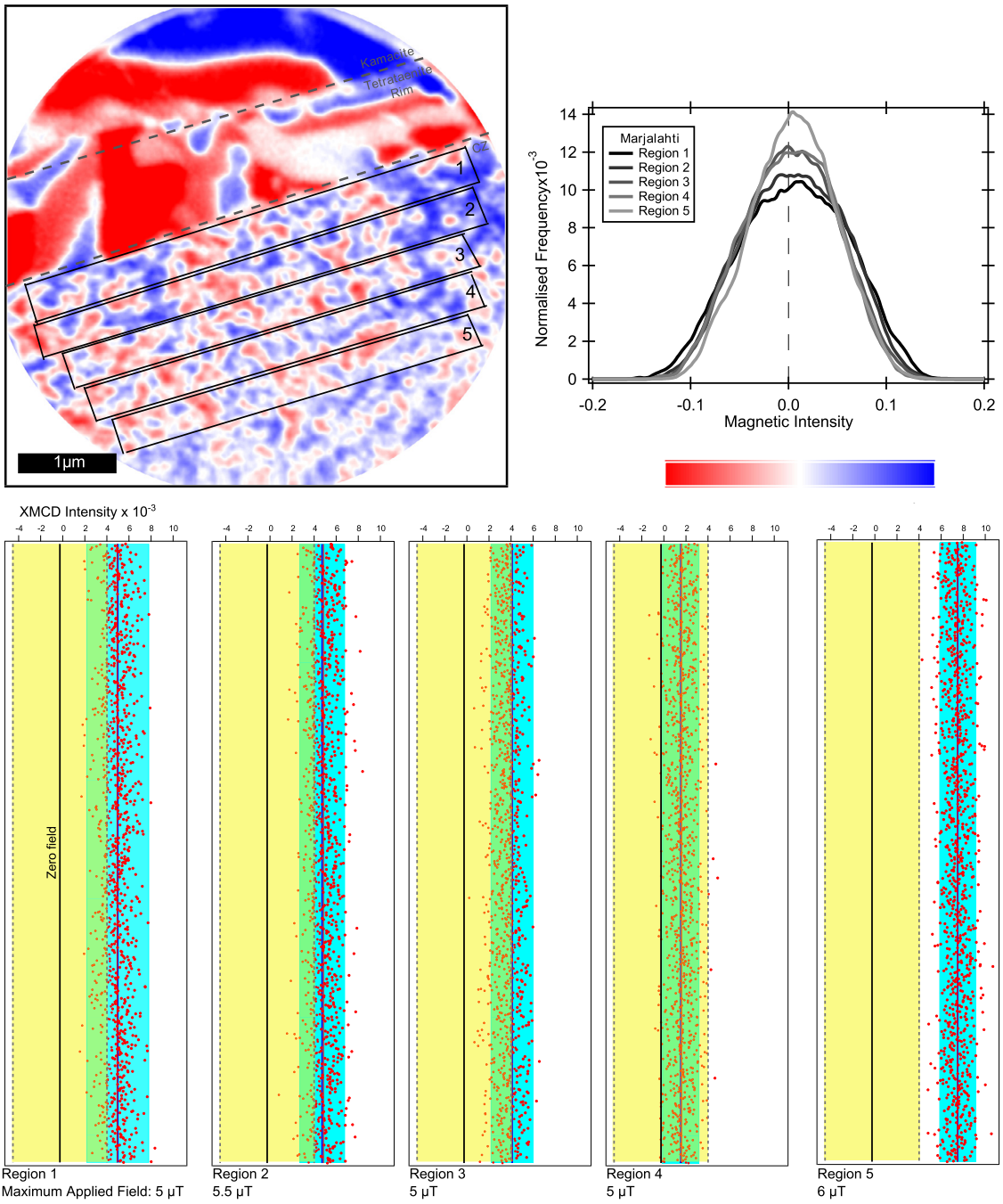

Fig. 4. An XMCD image for the Marjalahti shows the five regions analysed. The histogram shows the pixel intensity for the average of the 12 experimental images acquired and analysed. The lower five plots are the results of bootstraping analysis. The black line represents a simulation under zero ambient field. The yellow area represents 2 standard deviations, and hence describes a zero ambient field to a confidence level of 95%. The red dots represent the mean of the experimental histograms, resampled 1000 times. The blue line is the best fit to the experimental data, acquired by varying the ambient magnetic field. The pale blue region is the 95% confidence level for the maximum field fit. The maximum fit for each region is reported underneath each graph. (For interpretation of the references to colour in this figure legend, the reader is referred to the web version of this article.)

tised during the expected duration of the thermally driven core dynamo (Supplementary Fig. 3). M_{dyn} is the magnetic moment of the core dynamo. The moment of a thermal core dynamo is predicted to be $\sim 10^{16}$ A m^2, two orders of magnitude less than that predicted for a compositional dynamo (Bryson et al., 2015; Olson and Christensen, 2006). For a constant crustal thickness and crustal magnetic susceptibility (e.g., 10 km and 0.1 respectively) an order of magnitude increase in the dynamo moment will generate an order of magnitude increase in the internal field for constant crustal conditions; for example, for $M_{dyn} = 10^{16}$ A m^2 $B_{internal} =$ 0.0157 μT, whilst if $M_{dyn} = 10^{18}$ A m^2, $B_{internal} = 1.57$ μT. For a constant dynamo moment, crustal magnetic thickness and susceptibility both vary linearly with internal field.

The internal field value is also influenced by the relative permeability of the material, μ_r. For silicates, $\mu_r \sim 1$, whereas for kamacite, which makes up the majority of the FeNi metal in the pallasites, $\mu_r \sim 200$ (Brown, 1958). This relative permeability acts to amplify the intensity of the external field recorded by the cloudy zone. The degree of amplification depends on the morphology of the metal; two extremes in morphology are considered, a sphere

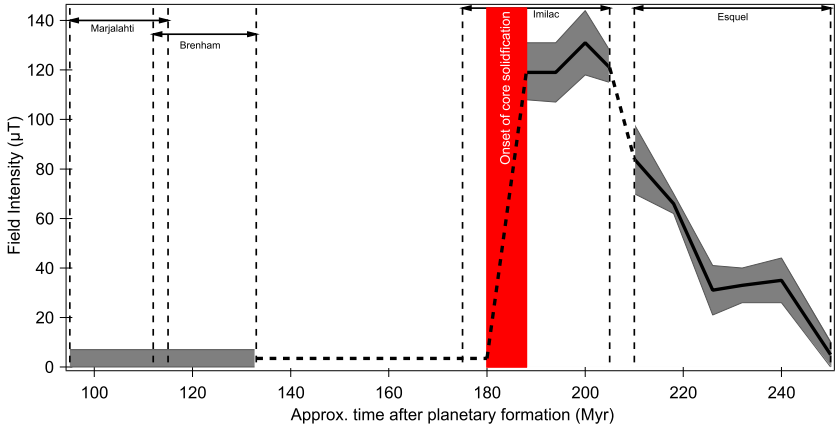

Fig. 5. Measured magnetic field intensity for the Marjalahti, Brenham, Imilac and Esquel pallasites. Results are time resolved based on the blocking temperature of tetrataenite and the cooling model for the Main Group pallasite parent body Bryson et al. (2015). The Marjalahti and Brenham record a weak magnetic field, ranging between ∼0 and 7 μT. This is thought to represent a quiescent period in core dynamo activity, and any weak magnetic field signal detected is attributed to a crustal remanence from early thermal dynamo activity. The onset of core solidification, represented by the red region is accompanied by the onset of a compositionally driven dynamo. This generates a strong magnetic field, as recorded by the Imilac. As core solidification continues, the field weakens and eventually the core dynamo 'switches off' when core solidification is complete. This 'dying' magnetic field is captured by the Esquel. (For interpretation of the references to colour in this figure legend, the reader is referred to the web version of this article.)

provides the weakest amplification factor of ∼3 whilst a rod generates an amplification factor of ∼200, if the external field is aligned directly along its length (Dunlop and Ozdemir, 1997). In the context of the MG pallasite parent body, a sphere is taken to represent an isolated pool of metal, whereas a rod represents a dyke intrusion. By considering the effects of amplification, we can say more about the relative timing of the pallasite-forming impact, and the morphology of the metal within the parent body.

The maximum internal field experienced by the Brenham and Marjalahti is shown in Fig. 6, for a range of plausible crustal thicknesses and crustal magnetic susceptibilities. The nature and abundance of crustal magnetic material in unknown, so we perform the calculations for a range of magnetic assemblages using empirically measured magnetisation values for typical ferromagnetic minerals (Kletetschka et al., 2006). A full range of plausible magnetic crustal susceptibilities is calculated by varying the type and amount of each magnetic phase present in the crust, assuming an average crustal density, $r_{crust} = 3200\ \mathrm{kg\,m^{-3}}$ (Johnson et al., 2015) (see Supplementary Table 3).

$$\chi_{TRM} = \frac{M \rho_{crust} f_i}{B/\mu_o} \tag{3}$$

M represents the magnetisation in $\mathrm{A\,m^2\,kg^{-1}}$ in a given field, B, and f_i is the fraction of magnetic material in the crust.

The typical magnetic susceptibility range for achondritic and chondritic crust is also shown (Fig. 6) based on susceptibility measurements from Rochette (2003) and Rochette et al. (2009). Based on the assumption that the MG pallasite parent body had a chondritic crust, this suggests that an amplification factor of ∼100–200 is required in order to explain the observed internal magnetic field. This is a larger degree of amplification than that required for the Imilac (by a factor of ∼10) but is in good agreement with the Esquel. Bryson et al. (2015) argue that variation in the degree of amplification may be caused by the pallasites coming from regions with different metal morphologies. Amplification may also vary depending on the orientation of metallic dykes to the dipolar field. Taking into account an amplification factor of ∼100–200, a weak magnetic field as recorded by the Brenham and Marjalahti can easily be explained by a crustal remanence induced by an early stage thermal dynamo.

The observed internal field values can also be explained by having a crust with a higher magnetic susceptibility than chondritic or achondritic crust; this could be achieved by having a crust with a higher metal content. A highly metallic crust could be formed by multiple impact events (such as the pallasite forming impact), covering the MG pallasite parent body in fragments of metal and silicate. The possibility of such impact events is supported by a drastic change in the cooling rate of the parent body as debris was supplied to its surface, insulating its interior. An initial fast cooling rate of the pallasites at high temperatures is evidenced by the wide range of metal–olivine equilibrium temperatures between 800 and 1200 °C (Reed et al., 1979; Scott, 1977), suggesting there was not time for Ni equilibration between the olivine and metal. The preservation of major and minor element zoning in the olivines also suggests the pallasites had a fast cooling rate of 20 to 100 °C per year from 1100–600 °C (Miyamoto, 1997). At lower temperatures, the cooling rate is much slower, suggesting impacts have deposited an insulating, regolith layer over the surface of the parent body. Evidence for slow cooling is the formation of the Widmanstätten pattern and associated microstructures, including the cloudy zone which, in the case of the pallasites forms at cooling rates of 2.5–18 $\mathrm{K\,Ma^{-1}}$. If the crust does have an unusually high magnetic susceptibility due to impact events, these events must have occurred before the thermal dynamo field 'switched off', <40 Ma after accretion (Ito and Ganguly, 2006). Therefore the observed magnetic field intensities can also be explained by a thermal dynamo-induced crustal remanence without amplification, if the crust has an unusually high magnetic susceptibility due to impact deposits.

4. Conclusions

The Marjalahti and Brenham main group pallasites were investigated in order to examine the relationship between composition and magnetisation in FeNi microstructures, and to constrain any paleomagnetic field signals captured by the samples. This is the first study to directly compare composition and magnetisation of the cloudy zone with nanoscale resolution. Within the cloudy zone, the islands are well resolved in compositional images and the boundary between islands and matrix is easily observed. The associated magnetisation pattern shows magnetic domains wrapping around clusters of island and matrix. This suggests that the matrix is ferromagnetic, and the islands and matrix are exchange coupled, rather than behaving independently. This supports the conclusions of Bryson et al. (2014b) that the matrix is ordered $Fe_{0.75}Ni_{0.25}$,

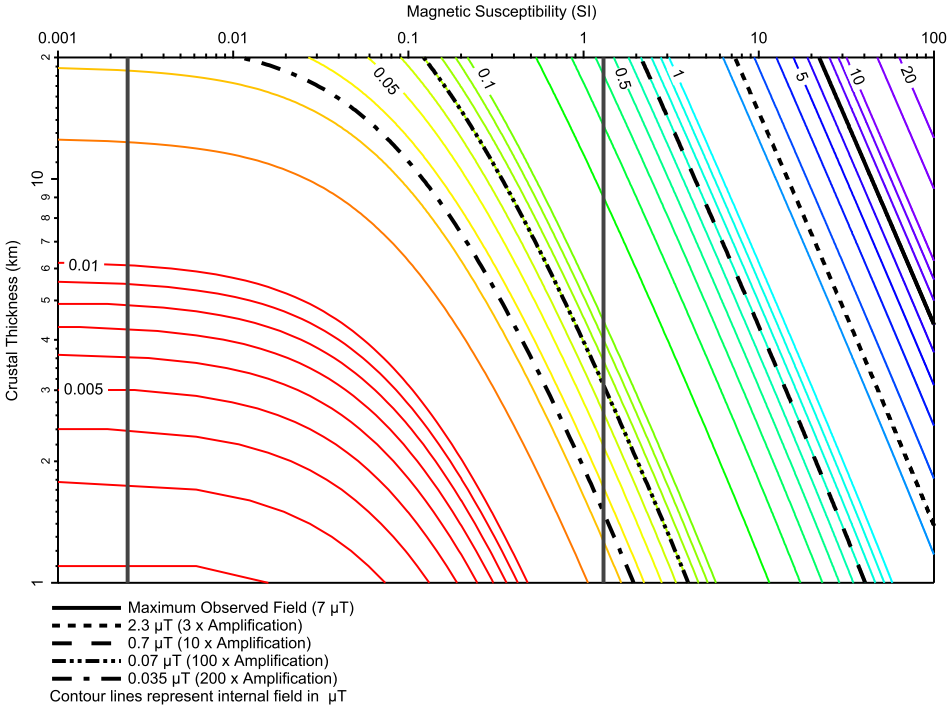

Fig. 6. The internal field experienced by the Brenham and Marjalahti pallasites, due to a crustal remanence imparted by an early thermal dynamo, is calculated for a range of crustal magnetic thickness and susceptibilities. The maximum crustal magnetic thickness is 20 km, based on the amount of crustal material that would have cooled through its Curie temperature by the time thermal dynamo activity ceased. The 'normal' range of crustal magnetic susceptibilities, calculated for achondritic and chondritic crust (Rochette, 2003; Rochette et al., 2009) is shown by the two grey, vertical lines. The Brenham and Marjalahti pallasites could have experienced internal fields of ~1–7 μT. Here we have plotted the maximum field (7 μT) as a solid black line. Various degrees of amplification are also considered and these are represented by the black dashed lines. The paleomagnetic fields experienced by the Brenham and Marjalahti can be explained by a chondritic or achondritic crustal composition if we assume a 100–200 deg of amplification, which could be caused by metallic dykes emplaced during the pallasite-parent-body-forming impact.

rather than antitaenite which is paramagnetic (Dos Santos et al., 2015).

The Brenham and Marjalahti have captured strikingly different paleomagnetic signals to the Imilac and Esquel. The Brenham and Marjalahti were specifically chosen based on their cooling rates, as they are predicted to have recorded a magnetic field prior to the onset of core solidification in the MG pallasite parent body. Compared to the Imilac and Esquel, which recorded strong paleomagnetic field signals induced by a compositional dynamo field, the weak field of the Brenham and Marjalahti can reasonably be explained as being caused by crustal remanence, left over from an earlier period of a thermally driven dynamo. The significant contrast in field strengths recorded by the pallasites suggests that core dynamos on small bodies vary temporally to a high degree and do not exhibit the same behaviour throughout their lifetimes. By furthering our understanding of the magnetic signals associated with each type of dynamo behaviour, paleomagnetic analyses can be used to constrain core behaviour in planetesimals, such as the onset of solidification and isothermal equilibrium within the core. A sharp change in magnetic field strength associated with the onset of core solidification may be a useful paleomagnetic signature to look for on Earth, and may provide invaluable help in establishing the age of the Earth's inner core, which is still poorly constrained (Labrosse et al., 2001; Nimmo and Alfe, 2007; Biggin et al., 2015).

Acknowledgements

We acknowledge the Helmholtz-Zentrum Berlin for the use of the synchrotron radiation beam time at beamline UE49 of BESSY II. The research leading to these results has received funding from the European Research Council under the European Union's Seventh Framework Programme (FP/2007–2013)/ERC grant agreement numbers 320750 and 312284, the Natural Environment Research Council and the Spanish MINECO project No. MAT2014-53921-R. We thank the Natural History Museum, London for samples.

Appendix A. Supplementary material

Supplementary material related to this article can be found online at http://dx.doi.org/10.1016/j.epsl.2016.02.037.

References

Asphaug, E., Agnor, C.B., Williams, Q., 2006. Hit-and-run planetary collisions. Nature 439 (7073), 155–160. URL http://www.ncbi.nlm.nih.gov/pubmed/16407944.

Biggin, A.J., Piispa, E.J., Pesonen, L.J., Holme, R., Paterson, G.A., Veikkolainen, T., Tauxe, L., 2015. Palaeomagnetic field intensity variations suggest Mesoproterozoic inner-core nucleation. Nature 526 (7572), 245–248. URL http://www.nature.com/doifinder/10.1038/nature15523.

Brown, W.F., 1958. Magnetic materials. In: Condon, E., Odishaw, H. (Eds.), Handbook of Chemistry and Physics. McGraw–Hill, New York, Ch. 8.

Bryson, J.F., Church, N.S., Kasama, T., Harrison, R.J., 2014a. Nanomagnetic intergrowths in FeNi meteoritic metal: the potential for time resolved records of planetesimal dynamo fields. Earth Planet. Sci. Lett. 388, 237–248. URL http://linkinghub.elsevier.com/retrieve/pii/S0012821X13007012.

Bryson, J.F., Herrero-Albillos, J., Kronast, F., Ghidini, M., Redfern, A.T.S., van der Laan, G., Harrison, R.J., 2014b. Nanopaleomagnetism of meteoritic FeNi studied using X-ray photoemission electron microscopy. Earth Planet. Sci. Lett. 396, 125–133. URL http://www.sciencedirect.com/science/article/pii/S0012821X14002489.

Bryson, J.F.J., Nichols, C.I.O., Herrero-Albillos, J., Kronast, F., Kasama, T., Alimadadi, H., Laan, G.V.D., Nimmo, F., Harrison, R.J., 2015. Long-lived magnetism from solidification-driven convection on the pallasite parent body. Nature 517 (7535), 472–475. http://dx.doi.org/10.1038/nature14114.

Chabot, N.L., 2004. Sulfur contents of the parental metallic cores of magmatic iron meteorites. Geochim. Cosmochim. Acta 68 (17), 3607–3618.

DiCiccio, T.J., Efron, B., 1988. Bootstrap confidence intervals. Stat. Probab. Lett. 7 (2), 151–160.

Dos Santos, E., Gattacceca, J., Rochette, P., Scorzelli, R., Fillion, G., 2015. Magnetic hysteresis properties and ^{57}Fe Mössbauer spectroscopy of iron and stony-iron meteorites: implications for mineralogy and thermal history. Phys.

Earth Planet. Inter. 242, 50–64. URL http://linkinghub.elsevier.com/retrieve/pii/S0031920115000217.

Dunlop, D.J., Ozdemir, O., 1997. Rock Magnetism: Fundamentals and Frontiers.

Dwyer, C.A., Stevenson, D.J., Nimmo, F., 2011. A long-lived lunar dynamo driven by continuous mechanical stirring. Nature 479 (7372), 212–214. URL http://www.ncbi.nlm.nih.gov/pubmed/22071766.

Elkins-Tanton, L.T., Weiss, B.P., Zuber, M.T., 2011. Chondrites as samples of differentiated planetesimals. Earth Planet. Sci. Lett. 305 (1–2), 1–10. URL http://linkinghub.elsevier.com/retrieve/pii/S0012821X11001543.

Garrick-Bethell, I., Weiss, B.P., 2010. Kamacite blocking temperatures and applications to lunar magnetism. Earth Planet. Sci. Lett. 294 (1–2), 1–7. http://dx.doi.org/10.1016/j.epsl.2010.02.013.

Goldstein, J.I., Michael, J.R., 2006. The formation of plessite in meteoritic metal. Meteorit. Planet. Sci. 41 (4), 553–570. URL http://doi.wiley.com/10.1111/j.1945-5100.2006.tb00482.x.

Hsu, W., 2003. Minor element zoning and trace element geochemistry of pallasites. Meteorit. Planet. Sci. 38 (8), 1217–1241. URL http://doi.wiley.com/10.1111/j.1945-5100.2003.tb00309.x.

Ito, M., Ganguly, J., 2006. Diffusion kinetics of Cr in olivine and ^{53}Mn–^{53}Cr thermochronology of early solar system objects. Geochim. Cosmochim. Acta 70 (3), 799–809.

Johnson, C.L., Phillips, R.J., Purucker, M.E., Anderson, B.J., Byrne, P.K., Denevi, B.W., Feinberg, J.M., Hauck, S.A., Head, J.W., Korth, H., James, P.B., Mazarico, E., Neumann, G.A., Philpott, L.C., Siegler, M.A., Tsyganenko, N.A., Solomon, S.C., 2015. Low-altitude magnetic field measurements by MESSENGER reveal Mercury's ancient crustal field. Science, 1–36. URL http://www.sciencemag.org/cgi/doi/10.1126/science.aaa8720.

Kletetschka, G., Fuller, M.D., Kohout, T., Wasilewski, P.J., Herrero-Bervera, E., Ness, N.F., Acuna, M.H., 2006. TRM in low magnetic fields: a minimum field that can be recorded by large multidomain grains. Phys. Earth Planet. Inter. 154 (3–4), 290–298.

Kronast, F., Schlichting, J., Radu, F., Mishra, S.K., Noll, T., Dürr, H.A., 2010. Spin-resolved photoemission microscopy and magnetic imaging in applied magnetic fields. Surf. Interface Anal. 42 (10–11), 1532–1536.

Labrosse, S., Poirier, J.P., Le Mouël, J.L., 2001. The age of the inner core. Earth Planet. Sci. Lett. 190 (3–4), 111–123.

Le Bars, M., Wieczorek, M.A., Karatekin, Ö., Cébron, D., Laneuville, M., 2011. An impact-driven dynamo for the early Moon. Nature 479 (7372), 215–218.

Lewis, L.H., Mubarok, A., Poirier, E., Bordeaux, N., Manchanda, P., Kashyap, A., Skomski, R., Goldstein, J., Pinkerton, F.E., Mishra, R.K., Kubic, R.C., Barmak, K., 2014. Inspired by nature: investigating tetrataenite for permanent magnet applications. J. Phys., Condens. Matter 26 (6), 064213. URL http://www.ncbi.nlm.nih.gov/pubmed/24469336.

Locatelli, A., Bauer, E., 2008. Recent advances in chemical and magnetic imaging of surfaces and interfaces by XPEEM. J. Phys. Condens. Matter 20 (9), 093002.

Miyamoto, M., 1997. Chemical zoning of olivine in several pallasites. J. Geophys. Res. 102 (E9), 21613.

Nimmo, F., 2009. Energetics of asteroid dynamos and the role of compositional convection. Geophys. Res. Lett. 36 (10), L10201. URL http://doi.wiley.com/10.1029/2009GL037997.

Nimmo, F., Alfe, D., 2007. Properties and evolution of the Earth's core and geodynamo. In: Advances in Science, pp. 1–39. URL http://discovery.ucl.ac.uk/48531/.

Nolting, F., Scholl, A., Stohr, J., Seo, J., Fompeyrine, J., Siegwart, H., Locquet, J., Anders, S., Luning, J., Fullerton, E., Toney, M., Scheinfein, M., Padmore, H., 2000. Direct observation of the alignment of ferromagnetic spins by antiferromagnetic spins. Nature 405 (6788), 767–769. URL http://www.ncbi.nlm.nih.gov/pubmed/10866191.

Ohldag, H., Regan, T., Stöhr, J., Scholl, A., Nolting, F., Lüning, J., Stamm, C., Anders, S., White, R., 2001. Spectroscopic identification and direct imaging of interfacial magnetic spins. Phys. Rev. Lett. 87 (24), 247201. URL http://link.aps.org/doi/10.1103/PhysRevLett.87.247201.

Olson, P., Christensen, U.R., 2006. Dipole moment scaling for convection-driven planetary dynamos. Earth Planet. Sci. Lett. 250 (3–4), 561–571.

Reed, S., Scott, E., Long, J., 1979. Ion microprobe analysis of olivine in pallasite meteorites for nickel. Earth Planet. Sci. Lett. 43 (1), 5–12.

Reimold, W.U., Gibson, R.L., 2006. The melt rocks of the Vredefort impact structure – Vredefort Granophyre and pseudotachylitic breccias: implications for impact cratering and the evolution of the Witwatersrand Basin. Chem. Erde 66 (1), 1–35.

Rochette, P., 2003. Magnetic classification of stony meteorites, 1: ordinary chondrites. Meteorit. Planet. Sci. 38 (2), 251–268. URL http://onlinelibrary.wiley.com/doi/10.1111/j.1945-5100.2003.tb00263.x/abstract.

Rochette, P., Gattacceca, J., Bourot-Denise, M., Consolmagno, G., Folco, L., Kohout, T., Pesonen, L., Sagnotti, L., 2009. Magnetic classification of stony meteorites, 3: achondrites. Meteorit. Planet. Sci. 44 (3), 405–427.

Runcorn, S., 1975. On the interpretation of lunar magnetism. Phys. Earth Planet. Inter. 10 (4), 327–335.

Scheinberg, A., Fu, R.R., Elkins-Tanton, L.T., Weiss, B.P., Stanley, S., in press. Magnetic fields on asteroids and planetesimals. In: Planetesimals: Early Differentiation and Consequences for Planets. Cambridge University Press, Cambridge, UK.

Scott, E.R.D., 1977. Pallasites – metal composition, classification and relationships with iron meteorites. Geochim. Cosmochim. Acta 41 (1969).

Sterenborg, M., Crowley, J.W., 2013. Thermal evolution of early solar system planetesimals and the possibility of sustained dynamos. Phys. Earth Planet. Inter. 214, 53–73. http://dx.doi.org/10.1016/j.pepi.2012.10.006.

Stöhr, J., Padmore, H.A., Anders, S., Stammler, T., Scheinfein, M.R., 1998. Principles of X-ray magnetic dichroism spectromicroscopy. Surf. Rev. Lett. 5 (6), 1297–1308.

Tarduno, J.a., Cottrell, R.D., Nimmo, F., Hopkins, J., Voronov, J., Erickson, A., Blackman, E., Scott, E.R.D., McKinley, R., 2012. Evidence for a dynamo in the main group pallasite parent body. Science (New York) 338 (6109), 939–942. URL http://www.ncbi.nlm.nih.gov/pubmed/23161997.

Uehara, M., Gattacceca, J., Leroux, H., Jacob, D., van der Beek, C.J., 2011. Magnetic microstructures of metal grains in equilibrated ordinary chondrites and implications for paleomagnetism of meteorites. Earth Planet. Sci. Lett. 306 (3–4), 241–252. URL http://linkinghub.elsevier.com/retrieve/pii/S0012821X11002147.

Weinbruch, S., Styrsa, V., Müller, W.F., 2003. Exsolution and coarsening in iron-free clinopyroxene during isothermal annealing. Geochim. Cosmochim. Acta 67 (24), 5071–5082.

Weiss, B.P., Elkins-Tanton, L.T., 2013. Differentiated planetesimals and the parent bodies of chondrites. Annu. Rev. Earth Planet. Sci. 41 (1), 529–560. URL http://www.annualreviews.org/doi/abs/10.1146/annurev-earth-040610-133520.

Yang, C., Williams, D., Goldstein, J., 1996. A revision of the Fe–Ni phase diagram at low temperatures (<400 C). J. Phase Equilib. 17 (6), 522–531.

Yang, J., Goldstein, J.I., Scott, E.R., 2010. Main-group pallasites: thermal history, relationship to IIIAB irons, and origin. Geochim. Cosmochim. Acta 74 (15), 4471–4492. URL http://linkinghub.elsevier.com/retrieve/pii/S0016703710002012.